

The role of twinning and stacking fault-induced plasticity on the mechanical properties of aluminum-lithium-graphene nanocomposites

Sara I. Ahmad, Atef Zekri & Khaled M. Youssef

To cite this article: Sara I. Ahmad, Atef Zekri & Khaled M. Youssef (2024) The role of twinning and stacking fault-induced plasticity on the mechanical properties of aluminum-lithium-graphene nanocomposites, *Nanocomposites*, 10:1, 91-107, DOI: [10.1080/20550324.2024.2319383](https://doi.org/10.1080/20550324.2024.2319383)

To link to this article: <https://doi.org/10.1080/20550324.2024.2319383>



© 2024 The Author(s). Published by Informa UK Limited, trading as Taylor & Francis Group.



Published online: 24 Feb 2024.



Submit your article to this journal [↗](#)



Article views: 617



View related articles [↗](#)




View Crossmark data [↗](#)



Citing articles: 1 View citing articles [↗](#)

The role of twinning and stacking fault-induced plasticity on the mechanical properties of aluminum-lithium-graphene nanocomposites

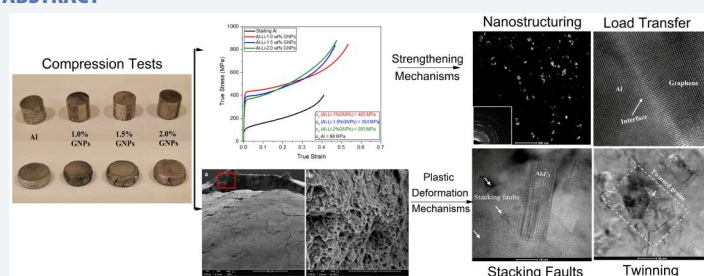
Sara I. Ahmad^{a,b}, Atef Zekri^b and Khaled M. Youssef^a 

^aMaterials Science and Technology Graduate Program, Department of Physics and Materials Science, Qatar University, Doha, Qatar; ^bQatar Environment and Energy Research Institute, Hamad Bin Khalifa University, Doha, Qatar

ABSTRACT

In this study, the synthesis-structure-property relationship of graphene-reinforced Al matrix nanocomposites was investigated. The Al-Li-GNPs nanocomposite was synthesized to attain both high strength and good ductility. The incorporation of GNPs as a reinforcement in the Al-based matrix provided a nanocomposite structure for an integrated strengthening effect. To promote plasticity and maintain good ductility, the nanocrystalline Al matrix was alloyed with Li to reduce its stacking fault energy and promote additional deformation mechanisms. The compressive yield strength (CYS) increased from 88 MPa for the starting Al to 403 MPa for the Al-Li-GNPs nanocomposites with 1.0 wt% GNPs. Fracture analysis indicated that the synthesized nanocomposite exhibited a ductile nature and significant plastic deformation. Based on microscopic analysis, the enhanced strength of the Al-Li-GNPs nanocomposite was attributed to grain refinement, load transfer, and strain hardening. The good ductility, on the other hand, was attributed to dislocation slipping, the formation of stacking faults, and twinning.

GRAPHICAL ABSTRACT



ARTICLE HISTORY

Received 31 October 2023
Accepted 12 February 2024

KEYWORDS



Aluminum; compression; graphene; mechanical properties; nanocomposites; plasticity; stacking faults; twinning

1. Introduction

Aluminum (Al) and its alloys remain the fastest-growing automotive and structural materials [1], and the design of novel Al-based materials to satisfy the high specific-strength requirements for light-weighting applications is gaining significant interest in the materials science field [2]. Pure Al has a tensile strength of ~ 90.0 MPa, which can be enhanced up to 700 MPa by alloying [3]. However, the addition of a large percentage of alloying elements can affect Al's density, workability, electrical and thermal conductivities, and corrosion resistance. The most commonly used Al alloy in transportation is A7075, which has an average tensile strength of ~ 540 MPa [4]. Harnessing the advantages of Al in modern technologies and advanced structures

requires a significant enhancement in its strength. Throughout the past years, several techniques have been investigated and successfully developed to induce significant enhancements to the mechanical strength and hardness of Al and its alloys.

In this regard, the nano-structuring of Al and its alloys and the synthesis of Al-based nanocomposites reinforced with graphene nanoplates (GNPs) are two widely investigated research fields for their promising capabilities to demonstrate a superior mechanical performance of Al [5–7]. On the one hand, nanocrystalline metals with reduced grain size (<100 nm) have proven experimentally to exhibit significantly higher mechanical strength and hardness compared to their microcrystalline counterparts, as described by the Hall–Petch relationship [8–10]. On the other hand, it has been reported that

CONTACT Khaled M. Youssef  kyoussef@qu.edu.qa  Materials Science and Technology Graduate Program, Department of Physics and Materials Science, Qatar University, Doha, Qatar

© 2024 The Author(s). Published by Informa UK Limited, trading as Taylor & Francis Group.

This is an Open Access article distributed under the terms of the Creative Commons Attribution License (<http://creativecommons.org/licenses/by/4.0/>), which permits unrestricted use, distribution, and reproduction in any medium, provided the original work is properly cited. The terms on which this article has been published allow the posting of the Accepted Manuscript in a repository by the author(s) or with their consent.

the superior mechanical properties of graphene [11] can be utilized in structural materials through the incorporation of GNPs as a nano-reinforcement into metal matrices such as Al to produce graphene-reinforced Al matrix composites (GRAMC) [12–18]. Khanna et al. [18] investigated the effect of different GNPs wt% on the mechanical properties of Al and reported $\sim 70\%$ and $\sim 73\%$ enhancement in compressive strength and hardness for their Al-0.5 wt%GNPs composite. Combining a nanocrystalline Al matrix with reinforcement for a combined strengthening mechanism has been investigated widely for ceramic-based reinforcements [19–22] but rarely for GNPs. Bhadauria et al. [21] reported an 85% and a 44% increase in the yield and ultimate tensile stresses, respectively, for a nanocrystalline Al/GNPs nanocomposite over the same composite when synthesized with a conventional micro-grained Al matrix.

Despite the reported mechanical strength enhancements, the majority of both nanocrystalline Al systems and GRAMC studies have reported a deterioration in plastic deformation and ductility [12,21–24]. Nanocrystalline metals have been associated with their limited work hardening capacity as restricted by their nanometric grain size, leading to failure just after yielding [24–26]. Similarly, the deterioration in ductility in GRAMC has been attributed to dislocation pinning by the GNPs reinforcement preventing further slipping and thus restricting further plastic deformation of the composites [12] with even some studies reporting a complete transfer from a ductile to a brittle fracture mode after the addition of GNPs [21,27]. Liu et al. reported a high yield strength of 260 MPa for their 80 nm grain-sized Al consolidated by spark plasma sintering (SPS) but with only 3.1% total elongation. Li et al. [28] reported a 4% tensile elongation for a GRAMC with 0.2 wt% GNPs from an original elongation of 11% for pure Al. Recent advancements in the synthesis and characterization procedures resulted in successful simultaneous enhancement in both strength and ductility of limited cases of nanocrystalline Al [29,30] and Al/GNPs nanocomposites [13,31–34].

When it comes to promoting plasticity and maintaining good ductility, tailoring the microstructure to encourage plastic deformation in Al is necessary. In general, dislocation slipping and twinning are the two competitive mechanisms for plastic deformation in metals [35,36]. In FCC Al, slipping is almost always dominant because the stress required to initiate dislocation slipping is far less than that required for twinning [35,37]. Nonetheless, Zhang et al. [38] observed through MDS a high density of deformation twins present in every grain in a

nanocrystalline Al system developed at a certain interatomic potential. The mechanism of formation of deformation twins was attributed to the emission of partial dislocations from the grain boundaries in nanocrystalline Al. Furthermore, Muzyk et al. [39] proved using density functional theory calculations that alloying Al with Li reduces its stacking fault energy and promotes the emission of partial dislocations, which in turn facilitates the formation of stacking faults and twinning planes. Experimentally, twinning has been observed in ball-milled, in-situ consolidated nanocrystalline Al-Li alloys [29]. Furthermore, because of its lower density, adding 1.0 wt% Li is reported to reduce Al's density by 3.0% [3,40]. Therefore, alloying Al with Li can induce both light-weighting of the Al-based matrix and activate deformation by twinning for an enhanced plastic deformation behavior.

It becomes apparent that the synthesis of an Al-based material with superior mechanical strength and good ductility requires careful consideration of the synthesis-structure-property relationship of that material. For this aim, we used reported literature to design and carefully tailor a novel nanocomposite material consisting of a nanocrystalline Al-Li matrix reinforced with GNPs using ball milling and hot pressing. The incorporation of graphene with Al-Li alloys has not been investigated or reported before despite the significant specific strength enhancements it provides. The ball-milling process in this study was set to serve several purposes: to alloy Al with Li, to achieve grain refinement of the Al-based matrix, and to homogeneously distribute the GNPs. Microstructural investigations were performed to determine the strengthening and deformation mechanisms in these Al-Li-GNPs nanocomposites. This study proves experimentally that ball-milled Al can achieve good deformation by forming stacking faults and nano-twins despite Al's relatively high stacking fault energy.

2. Materials and methods

2.1. Materials and synthesis of the Al-Li-GNPs nanocomposites

The starting material used in this study were gas-atomized pure Al powders (99.97% purity) with an average particle size of 15 μm purchased from Alfa Aesar, pure Li granules (99% purity) and graphene nanoplatelets (GNPs), both purchased from Sigma-Aldrich. Four different compositions were synthesized and investigated to study the effect of the GNPs content on the mechanical performance of the Al-0.5 wt% Li- x wt% GNPs nanocomposites, where $x = 0.5, 1.0, 1.5,$ and 2.0 . Only 0.5 wt% Li was added to induce light-weighting and activate the

deformation twinning in Al, all while remaining within the solid solubility of Li in Al [3,39].

All starting materials were kept and handled in the (MBRAUN LABstar) glovebox under an ultra-high pure (UHP) argon atmosphere ($O_2 < 0.5$ ppm). First, powders were weighed according to associated compositions, then loaded and sealed in a stainless-steel milling vial along with stainless-steel milling balls with a ball-to-powder ratio of 17:1 in the glove box. No process control agents (PCAs) were used. After loading the material, the milling vial was loaded in the high-energy SPEX 8000 shaker mill with a speed of 1725–1425 rpm and milled for 8 h. Milling was stopped for 10 min after every hour of milling to prevent overheating of the milling vial.

2.2. Mechanical testing of the Al-Li-GNPs nanocomposites

Hardness and compression tests were performed to investigate the mechanical performance of the Al-Li-GNPs nanocomposites. First, the as-milled Al-Li-GNPs powder was loaded in a tungsten carbide die in the glovebox under a UHP Argon atmosphere. The power was then hot-pressed under vacuum at 773 K and 500 MPa for 20 min into disks with a length/diameter (L/D) ratio of 1.0. The compression tests were conducted using (Lloyd Instruments universal tensile test machine LR 50Kplus) under a pressing rate of $0.36 \text{ mm} \cdot \text{min}^{-1}$. The hardness measurements were carried out using a (Future-Tech Microhardness Tester FM-800). A total of 8 indentations on each sample were performed using a 25 g load and a 10 s dwell time. For comparison, both hardness and compression tests were performed on the starting Al powder pressed using the same conditions as the Al-Li-GNPs nanocomposites.

2.3. Characterization of the Al-Li-GNPs nanocomposites

X-ray diffraction (XRD) spectrum of the nanocomposites was collected using a (PANalytical Empyrean Diffractometer) with a CuK α ($\lambda = 0.1542 \text{ nm}$) radiation. The XRD operating conditions were 45 kV, 40 mA, and 25 °C with a scanning range from 20° to 100°, a step size of 0.013°, and a scan rate of $0.044^\circ \text{ s}^{-1}$. The XRD line broadening was used to calculate the average grain size and lattice strain of nanocrystalline Al using the integral breadth analysis and the Averbach formula [41] shown below.

$$\frac{(\beta)^2}{\tan^2 \theta_o} = \frac{\lambda}{d} \left(\frac{\beta}{\tan \theta_o \sin \theta_o} \right) + 25 e^2 \quad (1)$$

Where β is the measured integral breadth, the full-width half maximum (FWHM) of the peak, θ_o

is the diffraction angle, λ is the x-ray wavelength for Cu K α of 0.154 nm, d is the average grain size, and e is the lattice strain. Raman spectra of the samples were obtained using a (Thermo fisher scientific DXR) with a laser wavelength of 532 nm to examine the structural integrity of the GNPs after milling. An average of three readings was obtained for each sample. Structural and morphological analyses were carried out using scanning electron microscopy (SEM) and transmission electron microscopy (TEM). The SEM images were acquired using an FEI Nova NanoSEM 450 operated at an accelerating voltage of 5.0 kV and a working distance of 5.0 mm. The TEM analysis was performed using a (Thermo Scientific TalosF200X TEM) operating at 200 keV to obtain selected area electron diffraction (SAED), bright-field (BF), dark-field (DF), and STEM-HAADF TEM images. The TEM samples were thinned down to a lamella using the (SEM/FIB Versa 3D dual beam, FEI) into a thickness between 25 nm and 75 nm.

3. Results

3.1. Effect of GNPs content on the milling of the Al-Li-GNPs nanocomposites

It is common practice to use a PCA or a surfactant during the milling of ductile metals such as Al to eliminate excessive welding and encourage fracturing and nano-structuring. However, such organic materials can present unwanted impurities in the milled powder and are not utilized in this study. Instead, the welding of the highly ductile Al powder is mitigated by the presence of GNPs. The self-lubricating nature of GNPs that stems from the weak van der Waals attraction forces between the graphene layers allows them to slide easily with respect to one another in between sliding surfaces [42], thus acting as a PCA. Therefore, the addition of GNPs to the Al-based matrix affects its performance and directly influences the success of its milling without powder welding.

Four different GNPs concentrations of 0.5, 1.0, 1.5, and 2.0 wt% were milled with the Al-Li in order to study the influence of the GNPs on the morphology of the ball-milled GRAMC. The SEM images in Figure 1(a,b,c) show the Al-Li-GNPs powder after milling for 8 h with 1.0, 1.5, and 2.0 wt% GNPs, respectively. The effect of the GNPs content on the particle size was evident in the SEM images, which showed a reduction in the particle size at higher GNPs content. The measured average particle size for the Al-Li-GNPs samples with 1.0, 1.5, and 2.0 wt% GNPs is $355 \pm 20 \mu\text{m}$, $244 \pm 20 \mu\text{m}$, and $224 \pm 10 \mu\text{m}$, respectively. Zhang et al. [43] observed a similar behavior of particle refinement with

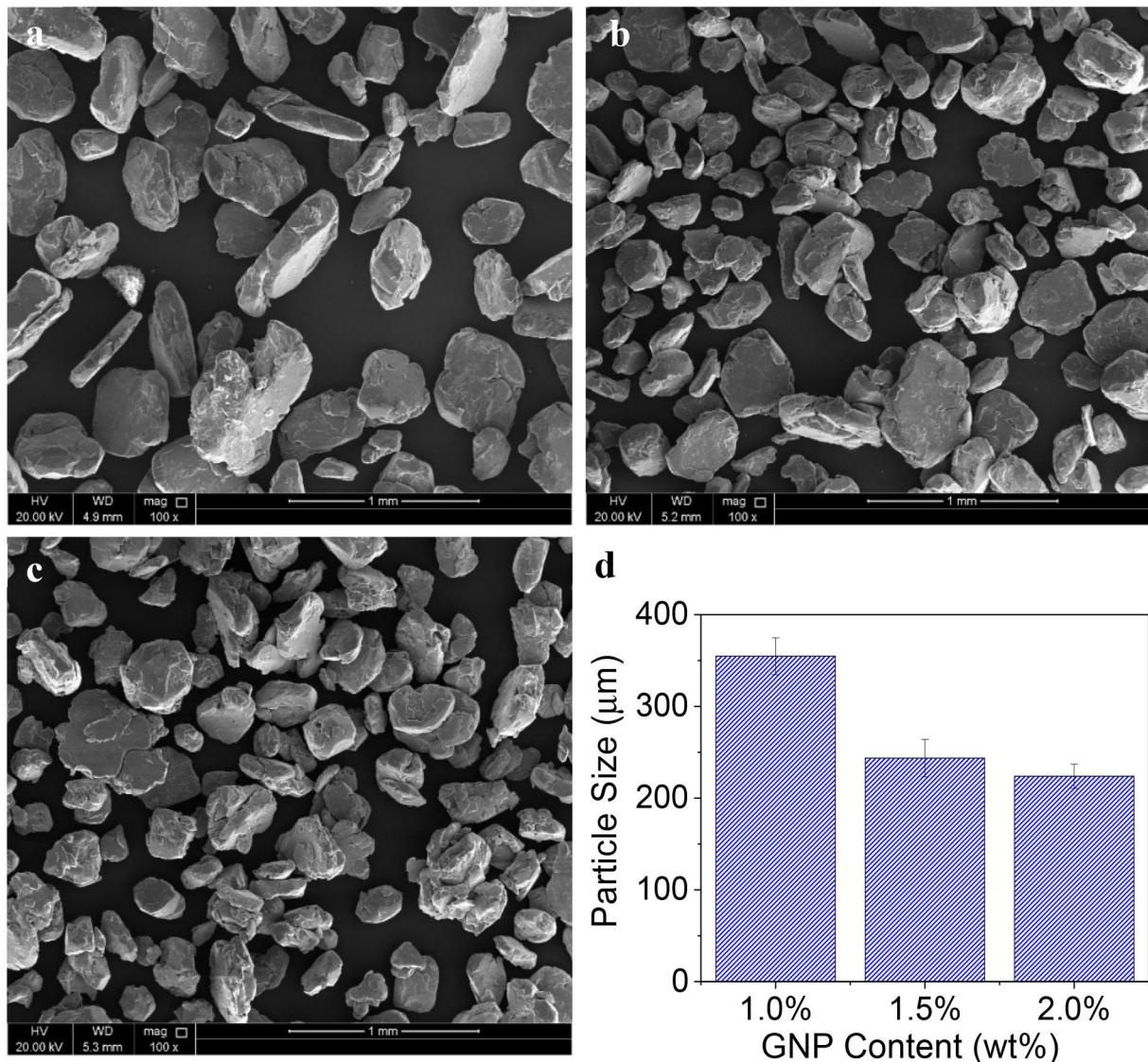


Figure 1. SEM images showing the morphology of the as-milled Al-Li-GNPs powder after 8 h of milling with (a) 1.0 wt%, (b) 1.5 wt%, and (c) 2.0 wt% GNPs. (d) Particle size of as-milled samples vs. GNPs content.

increasing GNPs content in a milled Al5083/GNPs nanocomposite and concluded that the addition of the GNPs accelerated the milling process.

Under the same milling conditions, complete welding of the Al-Li-GNPs sample occurred with 0.5 wt% GNPs content. After only 4 h of milling, the powder exhibited severe welding, and the entire sample formed a sheet stuck to the milling vial wall. It is concluded that 0.5 wt% GNPs was not enough to initiate cold-working of the Al powder and prevent its cold-welding and that the heat generated during milling and the ductility of Al far outweighed the lubrication of the 0.5 wt% of GNPs. These observations directly confirm the role of GNPs as a lubricant and the possibility of milling ductile metals such as Al at room temperature without using a PCA.

3.2. Effect of GNPs content on the microstructure and microhardness of the Al-Li-GNPs nanocomposites

The crystal structure, phase formation, and grain size of the Al-Li-GNPs nanocomposites with different GNPs content were investigated using the XRD patterns shown in Figure 2(a). As indexed on the XRD patterns, only FCC Al diffraction peaks were observed for all Al-Li-GNPs samples. No peaks were observed for Li second phases, affirming the effective alloying process during milling. No peaks for the GNPs were observed which could be related to the low content of GNPs beyond the XRD detection limit [20,44]. Furthermore, no peaks appeared for the Al_4C_3 even in samples with higher GNPs concentrations.

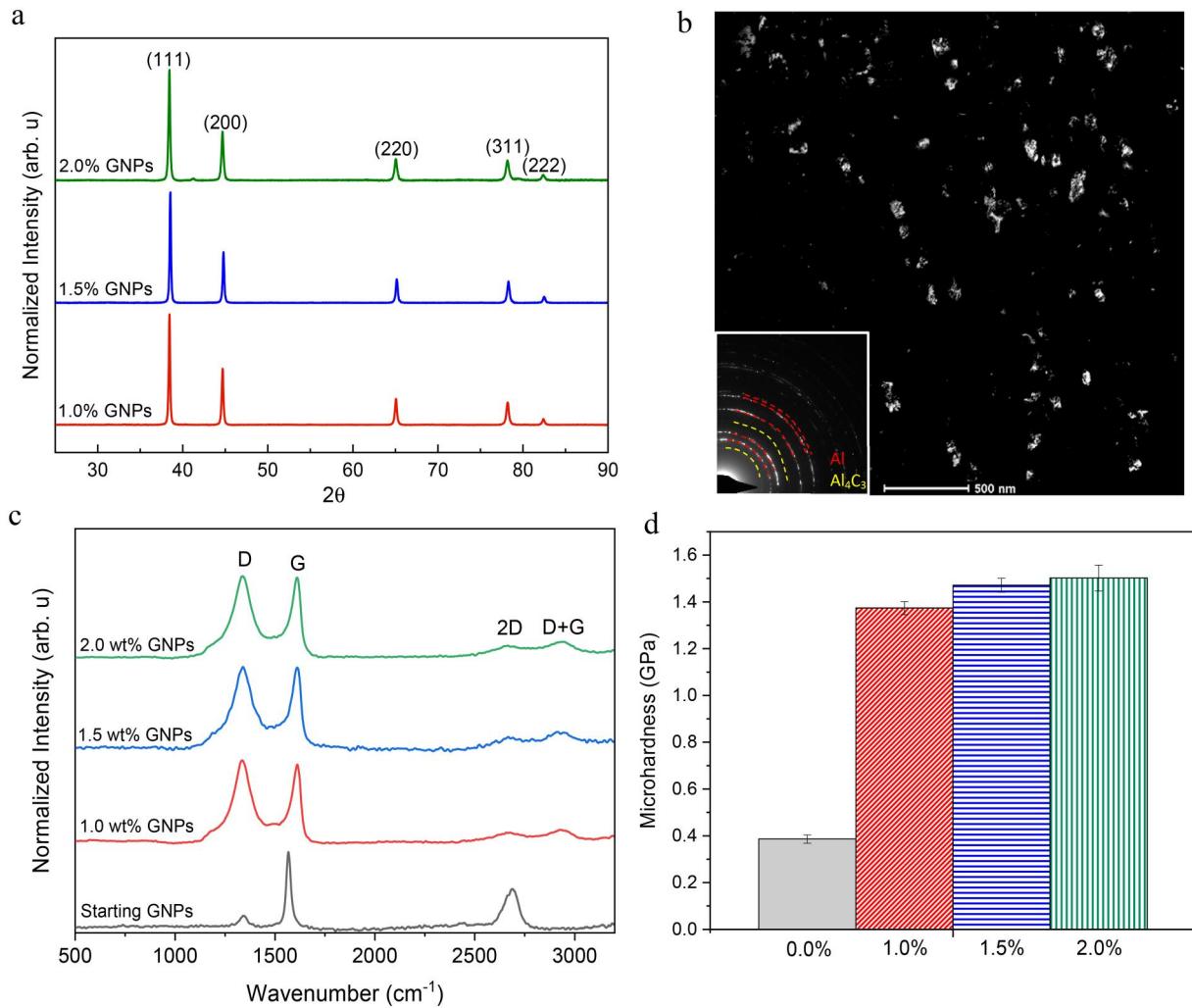


Figure 2. (a) XRD patterns, (b) dark-field TEM image and its corresponding SAED pattern of the Al-Li-2.0 wt% GNP nanocomposite, (c) Raman spectroscopy, and (d) Vickers microhardness of the Al-Li-GNPs nanocomposites with different GNPs content.

Table 1. Grain size, microhardness, and relative density of the Al-Li-GNPs nanocomposites.

Sample	XRD grain size (nm)	Microhardness (GPa)	CYS (MPa)	Relative density
Al-Li-1.0 wt% GNPs	59	1.37 ± 0.03	403 ± 20	98.9%
Al-Li-1.5 wt% GNPs	53	1.47 ± 0.03	354 ± 14	98.4%
Al-Li-2.0 wt% GNPs	37	1.50 ± 0.06	293 ± 11	98.6%

The average grain size for the Al-Li-GNPs nanocomposites with different GNPs content was calculated from the XRD patterns using the Averbach formula, see Table 1. The average grain size decreased from 59 nm for the Al-Li-1.0 wt% GNPs nanocomposite to 53 nm and 37 nm when the GNPs wt% was increased to 1.5 and 2.0 wt%, respectively. The addition of a nano-reinforcement, such as graphene sheets, has been reported to reduce the ductility of Al by pinning dislocations inside the metal lattice [12,43,45], causing the Al to fracture easier in the presence of larger GNPs content and yielding smaller grain sizes.

It is common practice to confirm the XRD average grain size calculations by TEM. The dark-field TEM image and its corresponding SAED pattern of the Al-Li-2.0 wt% GNPs sample are shown in Figure 2(b). The SAED rings are indexed to the Al FCC

phase. However, new lower-intensity rings appear in addition to the Al FCC rings, insinuating the presence of a second phase. These rings were indexed to the Al_4C_3 phase. Therefore, the absence of any Al_4C_3 peaks in the XRD patterns, as opposed to its detection in the SAED rings, can be related to its lower content beyond the XRD detection limit [21]. Based on measuring the size of 150 grains from the dark-field TEM image, the average grain size of the Al-Li-2.0 wt% GNPs nanocomposite was determined to be 42 nm, which is in agreement with the 37 nm average grain size calculated by the Averbach formula and the XRD pattern.

Raman spectroscopy is a non-destructive tool usually used to confirm the presence of GNPs and assess their structural integrity after milling. Raman spectra of the Al-Li-GNPs nanocomposites milled with different GNPs content are shown in Figure 2(c).

For comparison, the Raman spectra of the starting GNPs are included in Figure 2(c) as well. The Raman spectra of all samples present the characteristic graphene peak at around 1350 and 1580 corresponding to the D and G peaks, respectively [46,47]. The G-band is associated with sp^2 carbon structure and corresponds to the in-plane vibration of C-C bonds in a graphite lattice, while the D-band is associated with sp^3 lattice disorders and requires the presence of defects for its activation [46]. The intensity of the D-band increased significantly in the Al-Li-1.0 wt% GNPs nanocomposite after milling as compared to the intensity of the D band of pure GNPs, see Figure 2(c). The intensity ratio of the D-band to the G-band (I_D/I_G) is usually used to assess the degree of structural defects or disorders in sp^2 -based carbon structures and was found to increase from 0.14 for the starting GNPs, to 1.11, 1.02, and 1.07 for the Al-Li-GNPs with 1.0%, 1.5%, and 2% GNPs, respectively. The similar values of the I_D/I_G ratios of the three samples suggest that the GNPs content played little to no role in the extent of structural damage induced upon the graphene sheets during milling. It is important to note that the presence of a sharp G peak after 8 h of high-energy milling implies the presence of GNPs with high crystallinity and a preserved graphitic aromatic structure [46]. The I_D/I_G of ~ 1.00 in the ball-milled Al-Li-GNPs after milling is in good agreement with reported values for other GRAMCs synthesized by ball-milling [5]. In fact, Yu et al. [48] reported a higher I_D/I_G ratio of 1.42 for Al/GNPs composite milled for 7 h.

Microhardness measurements of the starting Al and the synthesized Al-Li-GNPs samples with different GNPs content are shown in Figure 2(d) and Table 1. The microhardness of the Al-Li-GNPs nanocomposites with 1.0, 1.5, and 2.0 wt% GNPs

was measured to be 1.37 ± 0.03 GPa, 1.47 ± 0.03 GPa, and 1.50 ± 0.07 GPa, respectively, significantly higher than that of the 0.38 ± 0.02 GPa measured for the starting Al. These results show that the microhardness values are higher in samples with higher GNPs content, which corresponds to the larger amount of reinforcement present in these samples. In addition, increasing the hardness values with increasing GNPs content is consistent with the XRD grain size calculations, which concluded that the grain size decreased with increasing GNPs content. Thus, these values confirm the integrated strengthening effect of both the GNPs as a reinforcement and grain refinement on the mechanical hardness of the Al-Li-GNPs nanocomposites. Thus far, both microstructural and microhardness analysis of the ball-milled and hot-pressed nanocomposites suggested the successful synthesis of a nanocrystalline Al-Li alloy reinforced with GNPs.

3.3. Compression tests of the Al-Li-GNPs nanocomposites

After hot-pressing, a relative density of 98.9%, 98.4%, and 98.6% was achieved for the Al-Li-GNPs nanocomposites with 1.0, 1.5, and 2.0 wt% GNPs, respectively. The Al-Li-GNPs hot-pressed disks are shown in Figure 3 before and after compression. As seen in Figure 3(b), definite flattening and bulging are observed in all samples after compression, along with cracks distributed along the circumference, see white arrows in Figure 3(b). These features are characteristic of ductile deformation under compression, suggesting that the synthesized Al-Li-GNPs nanocomposites underwent cold working and plastic deformation, and thus exhibited a ductile behavior. The compressive true stress-strain curves for the starting Al and the Al-Li-GNPs nanocomposites

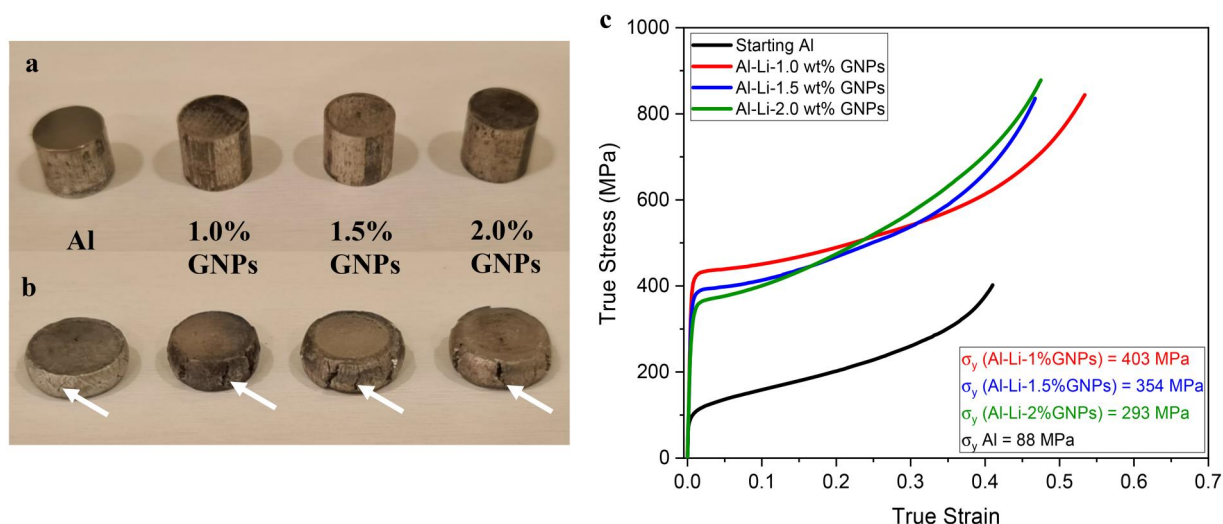


Figure 3. Al-Li-GNPs hot-pressed disks (a) before and (b) after compression tests. (c) Compressive true stress-strain curves of the starting Al, and the Al-Li-GNPs nanocomposites with 1.0 wt%, 1.5 wt%, and 2.0 wt% GNPs content.

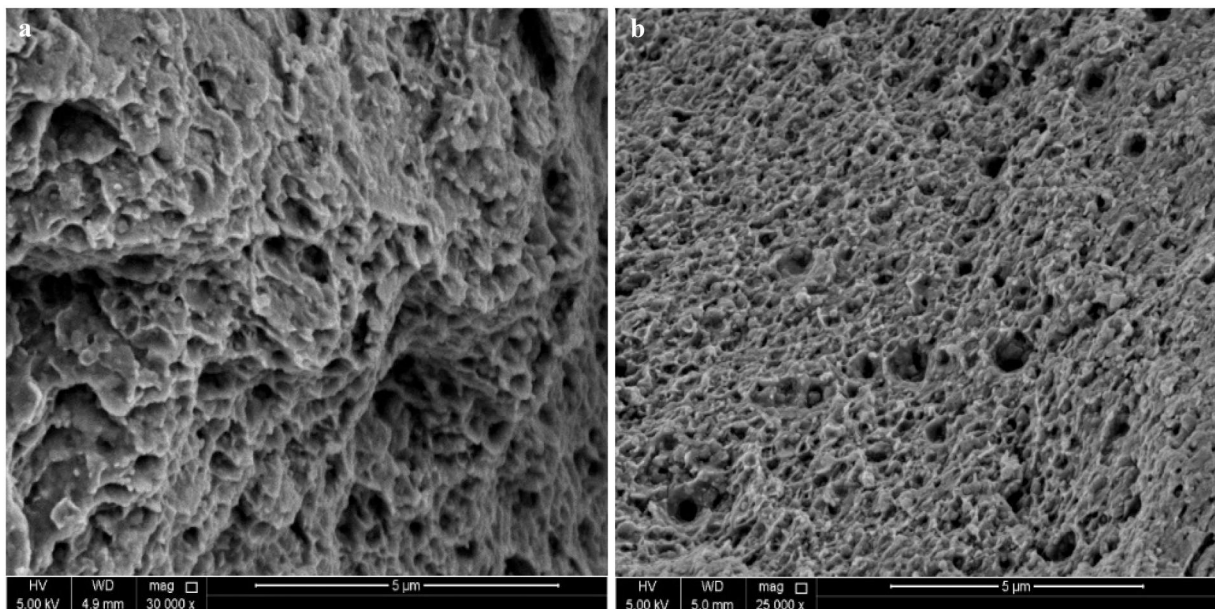


Figure 4. (a) and (b) SEM images taken from different areas of the compression fracture surface of the Al-Li-1.0 wt% GNPs nanocomposite.

with different GNPs content can be seen in [Figure 3\(c\)](#).

The CYS (σ_y) of the starting Al and the Al-Li-GNPs nanocomposites are presented in [Table 1](#). The CYS increased from 88 MPa for the starting Al to 293, 354, and 403 MPa for the Al-Li-GNPs nanocomposites with 2.0, 1.5, and 1.0 wt% GNPs, respectively. The CYSs of the Al-Li-GNPs nanocomposites are 3.3, 4.0, and 4.5 times higher than the CYS of the starting Al for the samples with 2.0, 1.5, and 1.0 wt% GNPs, respectively. It is apparent that the CYS increased significantly for the Al-Li-GNPs nanocomposites as compared to the starting Al. In addition, the yield strength of the Al-Li-GNPs nanocomposites started to drop with increasing the GNPs content.

The fracture surface of mechanically tested samples can yield information regarding their plastic deformation. The fracture surface of the Al-Li-1.0 wt% GNPs nanocomposite after compression can be seen in [Figure 4](#). Ductile fracture surfaces are characterized by the appearance of a rough dimple-like structure. During plastic deformation, voids nucleate at grain boundaries, slip planes, or interfaces, to accommodate the deformation incompatibility at these regions. These voids grow and coalesce with continued deformation, until, eventually, the interconnecting ligaments of the material separate, resulting in dimples [49,50]. Samples with little or no ductility exhibit smoother fracture morphology as little or no deformation occurs, and failure rather occurs by crack initiation and propagation. Therefore, the dimple-decorated ductile fracture surface observed in the SEM images in [Figure 4](#) suggests that the Al-Li-1.0 wt% GNPs sample

exhibited a considerable amount of plastic deformation before the final separation of the sample by localized shear [51].

4. Discussion

4.1. Mechanical behavior of the Al-Li-GNPs nanocomposites

As reported in [Figure 3](#) and [Table 1](#), the CYS of the ball-milled and hot-pressed Al-Li-GNPs nanocomposites increased significantly as compared to the starting Al, while at the same time, the yield strength of the Al-Li-GNPs nanocomposites started to drop with increasing the GNPs content. The detrimental effect on the mechanical properties of GRAMC at higher GNPs content has been reported widely [52,53], and is attributed to the agglomeration of the graphene sheets at higher GNPs content [53]. Therefore, the effect of GNPs agglomeration was higher than the strength induced by grain refinement at higher GNPs content [54]. Khan et al. [53] explored the effect of different GNPs loadings on the mechanical performance of an Al6061/GNPs composite. They reported an increase in the CYS from 236 MPa for the reference unreinforced sample to 257, 277, and 290 MPa after the addition of 0.1, 0.5, and 1.0 wt% GNPs, respectively. However, increasing the GNPs content to 3.0 wt% led to a sharp drop in the CYS to 220 MPa. The agglomeration of the thin sheets resulted in the formation of gaps and voids in between the agglomerated plates, which weakened the interface and deteriorated the mechanical performance of the nanocomposites.

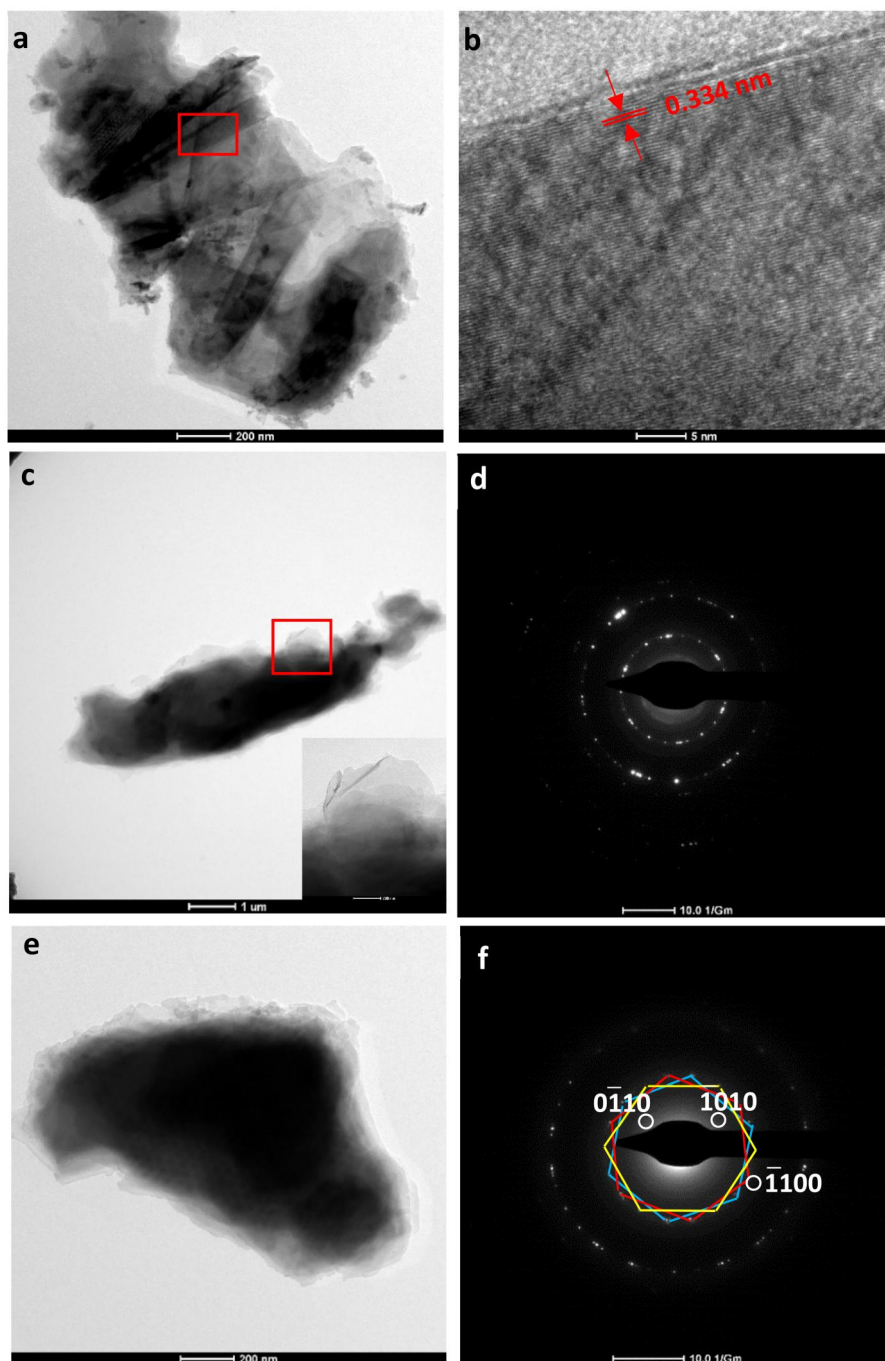


Figure 5. (a), (c), and (e) TEM images showing the stacking and agglomeration of the GNPs in the Al-Li-GNPs samples after milling with GNPs content of 1%, 1.5%, and 2%, respectively. (b) magnification of red box in (a), (d) SAED pattern of red box in (c), and (f) SAED pattern of (e).

TEM investigations can shed light on the structure and morphology of the GNPs in the samples after milling and help assess the degree of agglomeration. The TEM images in Figure 5 were taken for the as-milled Al-Li-GNPs samples with different GNPs content. The presence of a stacked and folded bundle of GNPs in the Al-Li-1.0 wt% GNPs sample can be seen in Figure 5(a). A magnification of Figure 5(a) is given in Figure 5(b), which confirms the crystallinity of the GNPs showing the planar (0002) graphene sheets with an interplanar spacing of 0.334 nm. Similarly, the stacking and agglomeration

of the GNPs are also seen in Figure 5(c,e) in the nanocomposites with 1.5 and 2.0 wt% GNPs, respectively. However, the TEM images indicate that the thickness of these bundles is larger at higher GNPs content. Graphene sheets are susceptible to agglomeration owing to their strong Van der Waals attraction forces. Thus, although mechanical milling has been proven efficient in exfoliating and dispersing the graphene sheets into metal matrices, the strong attraction forces, as well as the high energy circular vessel motion, allow the graphene sheets to easily wrinkle, fold, and agglomerate due to its remarkable

flexibility [28]. This behavior is shown in all samples containing GNPs, however the agglomeration and stacking appear to be larger in the samples with higher GNPs content.

The corresponding SAED patterns in Figure 5(d,f) confirm both the crystallinity and the stacking of the GNPs. The SAED pattern of graphene is characterized by its six-fold symmetry given its hexagonal crystal structure with a 120° angle between the reflected planes or spots [55]. Only six spots must appear if all the sheets are stacked with the same orientation. However, a rotation of the sheets would change the position at which the reflected spots appear due to the change in the orientation of the planes. Thus, the change in the orientation of a plane leads to a shift in the position of the corresponding spot but from the same distance from the center. The red, yellow, and blue hexagons in Figure 5(f) show some of the different diffraction patterns associated with different GNPs orientations, confirming the stacking and agglomeration of the GNPs in the samples.

In addition, the drop in the CYS can be attributed to the lower relative densities reported for the hot-pressed samples with higher GNPs content. The drop in density with increasing reinforcement content in aluminum matrix composites has been reported previously [12,56]. Gurbus et al. [56] reported a drop in the density of the Al composite with GNPs content above 0.1 wt%. This was attributed to the agglomeration tendency of GNPs at higher GNPs content, which reduced the contact area between the Al particles and prevented their rearrangement during pressing. Bisht et al. [12] reported a poor sinterability of the GNPs/Al composite at higher volume fraction addition of GNPs regardless of the sintering temperature.

This behavior differs from that of the microhardness reported in section 3.2 where the average microhardness values increased with increasing GNPs content. Microhardness measurements are less sensitive to porosities and relative densities than mechanical strength tests due to its localized testing areas. Thus, the lower relative densities with increasing GNPs content do not significantly affect the overall hardness of the nanocomposite. Nevertheless, the agglomeration of the GNPs at higher GNPs contents can still be deduced from hardness measurements. It can be seen in Figure 2(d) that the error bar is the highest for the hardness of the Al-Li-2.0 wt% GNPs content. This indicates the inhomogeneity of the microstructure and the agglomeration of the GNPs sheets across the sample at higher GNPs content. Similar behavior was observed by Hu et al. [57] in their GRAMC synthesized by ball-milling and 3D-printing.

4.2. Strengthening and deformation mechanisms

The enhancement in the mechanical strength of GRAMC is often attributed to several strengthening mechanisms, including grain refinement [58], load transfer [28,59], strain hardening and dislocation pinning [20,60], and the generation of dislocations due to the mismatch in the coefficient of thermal expansion (CTE) [21,61]. The contribution to the strengthening from each mechanism depends on the microstructures of the synthesized composites [62]. In this study, we rely on microscopic analysis to investigate the possible contributing strengthening mechanisms responsible for the significant enhancement in the strength and hardness of the ball-milled Al-Li-GNPs nanocomposites and their good ductility.

First, grain refinement is established as a main strengthening mechanism of metals, as indicated by the Hall-Petch relationship [63]. It is attributed to the introduction of a high density of grain boundaries, which act as obstacles preventing the dislocation motion, hindering deformation, and significantly enhancing the strength of nano-grained matrices [64,65]. The nanometric grain sizes obtained from the XRD calculations proved the successful nano-structuring of the ball-milled Al-Li-GNPs nanocomposites, see Table 1.

Second, the strengthening by the load transfer mechanism in GRAMCs, which is explained by the modified shear-lag model [66], is the main reason behind the incorporation of graphene in MMCs. During a mechanical test, the load is transferred from the plastically deformed matrix to the GNPs by shear stresses generated along their interface [67]. This strengthening mechanism has been confirmed experimentally in GNPs/Al composites where the GNPs were often found to exist in the dimples of the fracture surfaces of the GNPs/Al composites [28,58,68,69], indicating the load-bearing capability of the GNPs up until final fracture of the composite. Zhou et al. [69] performed an in-situ TEM bending test to observe the crack propagation and the role of the GNPs in a GNPs/Al composite. A graphene sheet was found to exist across the crack, acting as a bridge retaining the crack growth until the graphene sheet finally failed from the middle, which is a sign of enhanced interfacial bonding.

The load transfer efficiency is directly correlated to the integrity of the interfacial strength and bonding between the Al matrix and the GNPs [20]. The presence of a coherent, strong, and clean interface that is free of any voids or cracks between the Al lattice and a graphene sheet is shown in the HRTEM image taken for the Al-Li-2.0 wt% GNPs sample, see Figure 6. The high magnification HRTEM image in Figure 6(d) shows the preserved

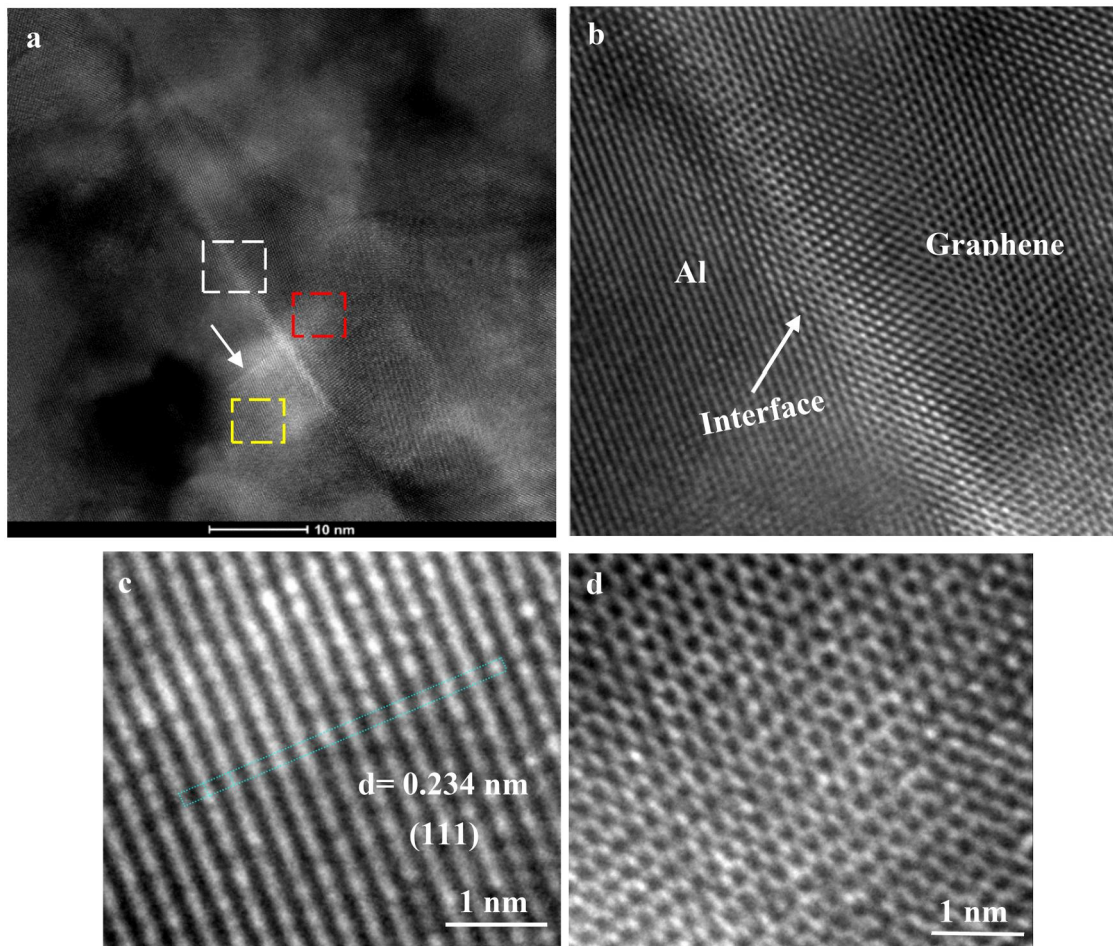


Figure 6. (a) A HRTEM image of the Al-Li-2.0wt% GNPs nanocomposite showing the interface between the Al matrix and the GNPs. (b), (c), and (d) magnification of white, yellow, and red boxes in (a), respectively.

honeycomb structure of the GNPs embedded in the Al matrix. The well-bonded interface is evidence for the efficient mixing of the GNPs in the Al matrix during ball-milling and the contribution of the load transfer mechanism in the ball-milled Al-Li-GNPs nanocomposites.

Furthermore, it has been reported that the strength of the interfacial bonding, and thus, the load transfer efficiency between the metal matrix and graphene can be enhanced by the Al_4C_3 partial interfacial reaction in Al matrices [62,70] and the use of defective low-quality graphene as a reinforcement [71]. Li et al. [62] investigated the tensile fracture surface of a 2.0 wt% GNPs/Al composite synthesized by ball-milling, cold drawing, and annealing. They observed that the GNPs in the as-drawn and 600°C annealed nanocomposites were pulled out, while the GNPs appeared fractured in the samples annealed above 600°C . They attributed the pull-out de-bonding phenomenon to the weaker interfacial bonding at lower temperatures and the fracture of the GNPs to the stronger interfacial bonding caused by the presence of the Al_4C_3 interfacial phases between the Al matrix and the GNPs at higher temperatures. The partial Al/GNPs reaction and the in-situ formation of the Al_4C_3 in the

Al-Li-GNPs nanocomposites are revealed in the TEM image in Figure 7(a). The HR-TEM image shows the interfacial relationship between the Al lattice and the Al_4C_3 rod-like nanoparticle, indicating a coherent chemical bonding which contributes to the enhancement of the load bearing capacity.

Strain-hardening or grain boundary dislocation pinning is another major strengthening mechanism in materials [72,73]. In graphene-reinforced nanocrystalline Al nanocomposites, the high density of grain boundaries in the nano-grained matrix act as obstacles to dislocation motion, preventing the continuous slip and propagation across the boundaries from one grain to the other, thus enhancing the strength of composites [2]. At the same time, the GNPs reinforcement and the Al_4C_3 second phase can effectively prevent the diffusion of atoms and prevent the dislocation motion, thus strengthening the Al matrix [14,52,67,68,70,74]. Furthermore, the mismatch in the coefficient of thermal expansion (CTE) between the GNPs ($1.0 \times 10^{-6} \text{K}^{-1}$) and the Al matrix ($23.6 \times 10^{-6} \text{K}^{-1}$) at the interface is reported to induce additional strain and cause the generation of a large number of dislocations, rendering the mismatch in the CTE a non-direct mechanism to enhance the strength and hardness of

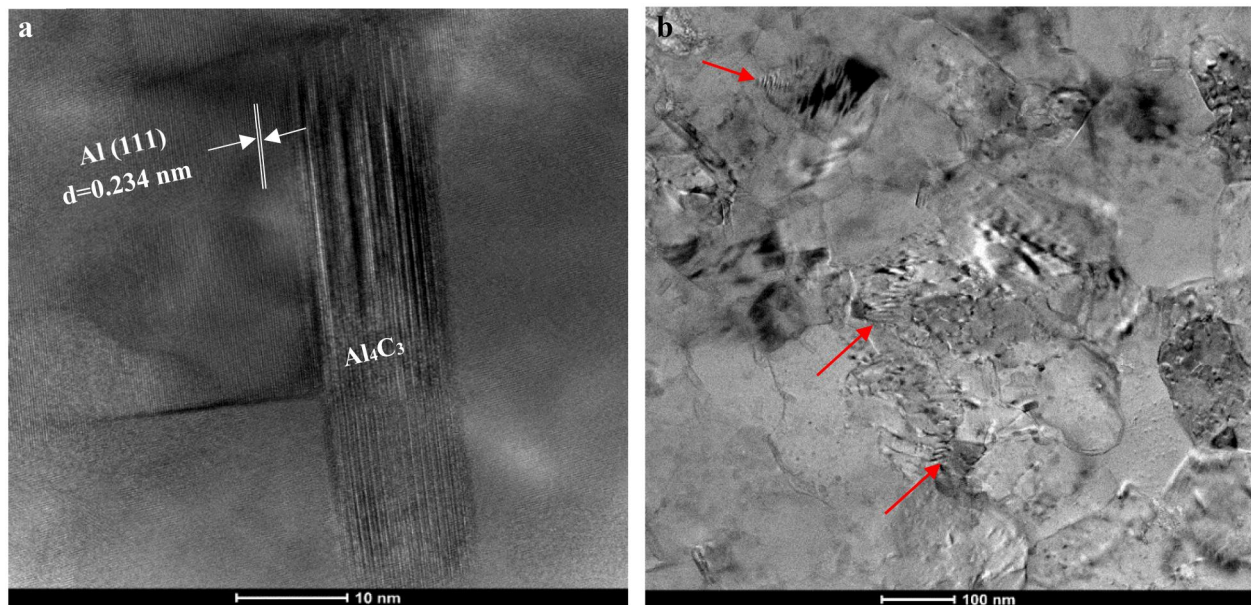


Figure 7. (a) A HRTEM image showing an Al_4C_3 nanoparticle forming a coherent interface with the Al matrix in the Al-Li-2.0 wt% GNPs nanocomposite, and (b) TEM image showing a high density of dislocations and dislocation cells distributed in the Al-Li-2.0 wt% GNPs nanocomposite.

GRAMCs [20,62,68,70,75]. Regardless of the origin of dislocations, the synthesized Al-Li-GNPs nanocomposites attained a high density of dislocations; see the BFTEM images in Figure 7(b,c). This is deemed of significant interest as it is generally accepted that nanocrystalline metals have limited work hardening capacity as restricted by their nanometric grain size [24–26]. Thus, the contribution from strain hardening and dislocation pinning to the strengthening of the ball-milled Al-Li-GNPs nanocomposites cannot be ignored. Based on the above analysis, the significant enhancement in the strength and hardness of the ball-milled Al-Li-GNPs nanocomposites can be attributed to the contribution of several strengthening mechanisms such as grain refinement, load transfer between the Al-based matrix and the GNPs, and dislocation strengthening/pinning or strain hardening.

In this study, the enhancement in the strength and hardness of the synthesized ball-milled Al-Li-GNPs nanocomposites was accompanied by good ductility and plastic deformation, as indicated by the SEM fracture surface images in Figure 4. This is deemed especially significant considering both the previously reported effects of the GNPs on the ductility of Al composites and the nanocrystalline nature of the ball-milled GNPs reinforced Al-Li nanocomposites. The majority of GRAMCs studies have reported a deterioration in the plastic deformation and the ductility of composites [12,21,28,33,43,61]. This behavior has been attributed to dislocation pinning by the reinforcement, preventing further slipping and thus restricting further plastic deformation of the composites [12]. Similarly, nanocrystalline metals have been associated with their

limited work hardening capacity, which is restricted by their nanometric grain size, leading to failure just after yielding [25]. Recent advancements in the synthesis and characterization procedures resulted in successful simultaneous enhancement in both strength and ductility of limited cases of nanocrystalline Al [29,30] and Al/GNPs nanocomposites [13,31–34].

In general, dislocation slipping and formation of twinning planes are the two competitive mechanisms for plastic deformation in metals. The domination of each mechanism is dependent upon the crystal system, the grain size, and the deformation conditions [35,36]. In FCC Al, slipping is almost always dominant because the stress required to initiate dislocation slipping is far less than the stress required for twinning [35]. Despite the small grain sizes, the abundance of dislocation pile-ups and dislocation cells have already been observed in the TEM images of the annealed Al-Li-GNPs nanocomposites, as seen in Figure 7(b,c). This could render dislocation generation and slipping the primary plastic deformation mechanism in the Al-Li-GNPs nanocomposites.

It is known that conventional coarse-grained Al has a high stacking fault energy which renders its deformation by twinning challenging [76,77]. In this regard, Muzyk et al. [39] proved using density functional theory calculations that alloying Al with Li reduces its stacking fault energy and promotes the emission of partial dislocations, which in turn facilitates the formation of stacking faults and twinning. A high concentration of stacking faults in the Al matrix is shown in the TEM images in Figure 8. In this study, Li was added to the Al to reduce its

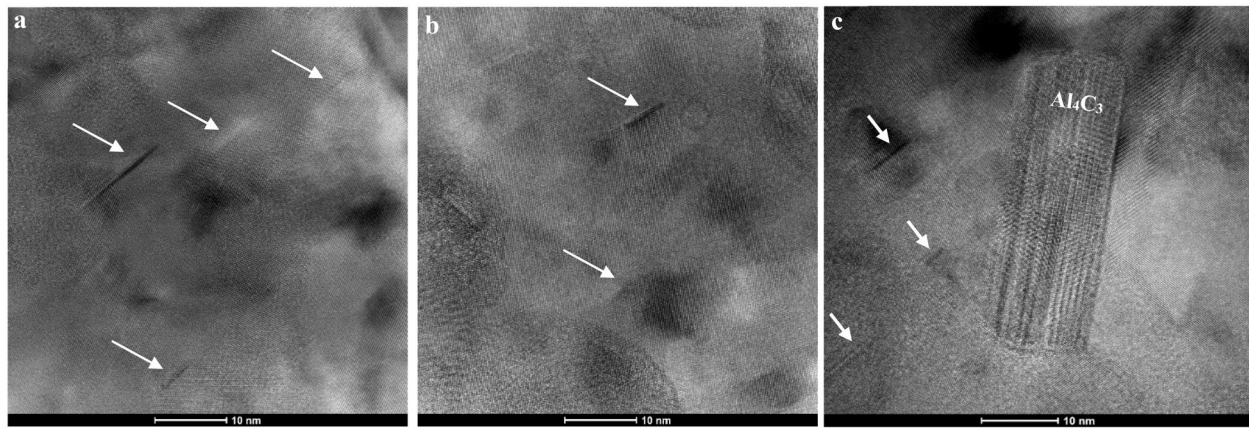


Figure 8. TEM images showing the presence of a large number of stacking faults in the ball-milled (a) Al-Li- 1.0 wt% GNPs and (b) Al-Li-2.0 wt% GNPs nanocomposites, and (c) a HRTEM image showing the presence of stacking faults around an Al_4C_3 nanoparticle.

stacking fault energy. Such Li solute atoms segregate to the stacking fault plane and increase the separation of partial dislocations around the stacking faults. This extended separation hinders the motion of the full dislocation and contributes to the overall strengthening observed in Figure 3(c) [78]. The observed high concentration of stacking faults in the Al matrix can also contribute to the good ductility of the Al-Li-GNPs through promoting deformation by twinning.

Experimentally, twinning has been observed in ball-milled in-situ consolidated nanocrystalline Al-Li alloys [29]. Furthermore, recent experimental and computational studies have reported the formation of stacking faults and twinning planes in GNPs/Al composites [28,79–82]. Li et al. observed the presence of nano twins and stacking faults in a GNPs/Al composite with 0.7 wt% GNPs synthesized by ball-milling, SPS, and hot extrusion [79], and in a GNPs/Al composite with 2.0 wt% GNPs synthesized by ball-milling, casting, and rolling [28]. They reported that the stacking faults were mostly distributed inside the Al grains near a GNPs/Al interface. Li et al. [80] used first-principle calculations to investigate the effect of GNPs on the stacking fault energy of the Al matrix. They found a significant decrease of 25.3% and 40.6% in the unstable and stable stacking fault energy, respectively, near the GNPs/Al interface. These conclusions are consistent with the TEM observations in Figure 8. In addition, the TEM image showing the coherent Al/GNPs interface in Figure 6(a) shows the presence of a stacking fault adjacent to the Al/GNPs interface, see white arrow.

Moreover, stacking faults adjacent to the Al_4C_3 nanoparticles can be occasionally observed in the Al-Li-GNPs nanocomposites, see Figure 8(c). Recently, Yang et al. [83] demonstrated that an interface between a rigid nanoparticle such as SiC and the Al matrix instead of grain boundaries, can

promote the formation of stacking faults in large-grained Al composites. They suggested that the atoms surrounding the Al/SiC interface can move even more easily than the atoms in the grain boundaries, generating partial dislocation, considering that the SiC nanoparticles are more rigid than Al. Therefore, it is apparent that the stacking fault energy of Al in the Al-Li-GNPs nanocomposites was reduced by a combined effect of all the elements present in the nanocomposite, the Li alloying element, the GNPs reinforcement, and the Al_4C_3 nanoparticles, which facilitated the plastic deformation by twinning.

In addition to stacking faults, another interesting twinning-related feature is observed in the TEM image in Figure 9; see the dashed white box. The image shows two Al grains exhibiting high symmetry, with one grain being the mirror image of the other, giving rise to a butterfly-like morphology. This type of symmetry is often referred to as twinning, and the surface along which the lattice points are shared in twinned grains is referred to as a twin plane or a twin boundary. The corresponding fast Fourier transformed (FFT) diffraction pattern from the twin boundary is shown as an inset in Figure 9. Due to their high symmetry, these interfaces attain much lower energy than the grain boundaries that form when grains grow with highly different orientations leading to a large atomic disorder at the boundaries. The driving force to reduce the stored strain, along with the reduced lower stacking fault energy of the system, enabled the formation of twinned boundaries instead of the conventional highly disordered grain boundaries. Similar twinned grain structures are rarely reported but have been observed by Li et al. [84] and Zhou et al. [85] for high entropy alloys and nanocrystalline Al-Mg alloys, respectively. In these cases, the formation of the twinned grains has been attributed to the

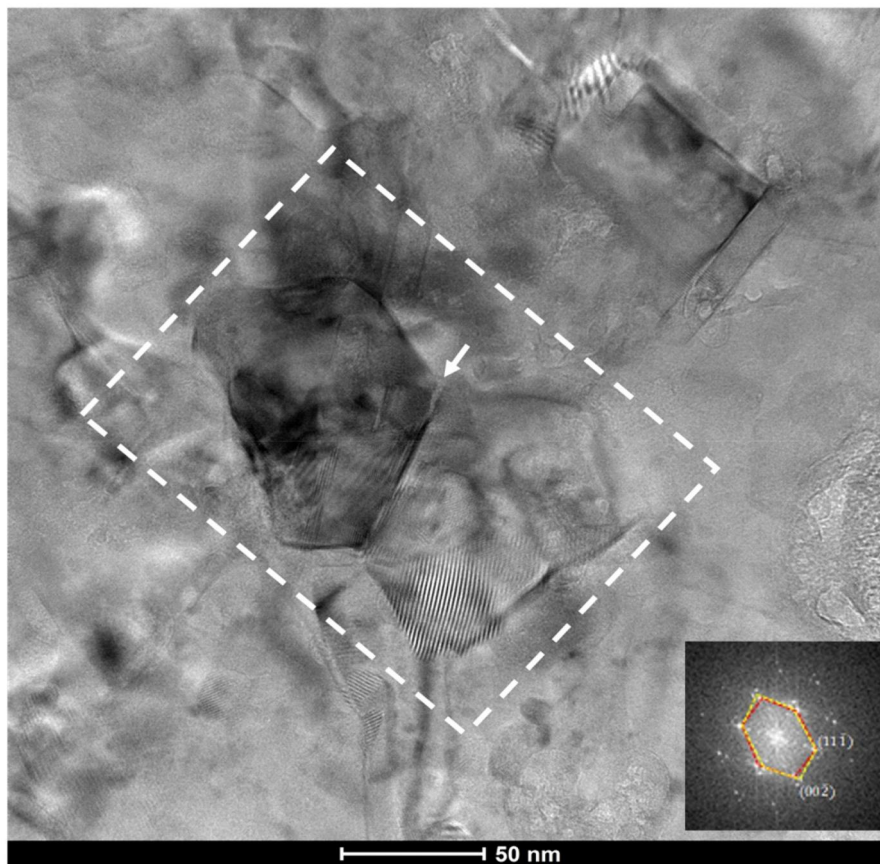


Figure 9. A TEM image showing the formation of twinned crystals in the Al-Li-1.5 wt % GNPs nanocomposite. Insert: the corresponding fast Fourier transformed (FFT) diffraction pattern from the twinned region.

recrystallization of the grain and the rearrangement of atoms after annealing.

These findings confirm that twinning, although a non-favorable deformation mechanism in conventional FCC Al because of its high stacking fault energy, is actually a preferred deformation mechanism in the synthesized ball-milled Al-Li-GNPs nanocomposites [38]. Finally, it is important to mention that although stacking faults and twinning planes help activate plastic deformation and thus enhance the ductility, it is also an important strengthening mechanism that could be added to those previously discussed. Stacking faults and twinning planes are reported to act as effective barriers to dislocation slip, thus contributing to the strain-hardening ability of materials and enhancing the strengthening of the nanocomposite [65,78,81,86].

Although it was mostly demonstrated in hardness and compression strength modes so far, it is clear that the enhancement in the mechanical performance of the synthesized Al-Li-GNPs nanocomposites with respect to the monolithic Al in the current study, in addition to its good plastic deformation behavior, is superior to other reported GRAMCs [20,52,87–90]. At this point, it becomes clear that the specific design and tailoring of the constituents

of this Al system allowed it to attain specific structural features, which significantly enhanced its performance.

5. Conclusion

In this study, the synthesis-structure-property relationship of graphene-reinforced Al-Li matrix nanocomposites was investigated. Ball milling was used to synthesize a GNPs reinforced Al-0.5 wt% Li matrix nanocomposite. The incorporation of GNPs as a reinforcement in the nanocrystalline Al-based matrix provided an integrated strengthening effect, while alloying the Al with 0.5 wt% Li promoted plasticity and good ductility. The yield strength increased from 88 MPa for the starting Al to 403 MPa for the Al-Li-GNPs nanocomposites with 1.0 wt% GNPs. Fracture analysis indicated that the synthesized nanocomposite exhibited a ductile nature and significant plastic deformation. Based on microscopic analysis, the enhanced strength of the Al-Li-GNPs nanocomposite was attributed to grain refinement, load transfer, and strain hardening. The good ductility, on the other hand, was attributed to dislocation slipping, the formation of stacking faults, and twinning.

Acknowledgments

The authors would like to acknowledge the technical support provided by Qatar Environment and Energy Research Institute (QEERI), and the Central Laboratory Unit (CLU), and the Center of Advanced Materials (CAM) at Qatar University.

CRedit authorship contribution statement

Sara I. Ahmad: Conceptualization, Data curation, Formal analysis, Investigation, Methodology, Validation, Visualization, Writing – original draft. **Atef Zekri:** Resources, Investigation. **Khaled M. Youssef:** Conceptualization, Investigation, Methodology, Funding acquisition, Project administration, Supervision, Writing – review & editing.

Disclosure statement

No potential conflict of interest was reported by the author(s).

Funding

This work was made possible by NPRP Grant no. NPRP11S-1203-170056 from the Qatar National Research Fund (a member of the Qatar Foundation) and The IRCC Grant no. IRCC-2021-008 from Qatar University. Open Access funding is provided by the Qatar National Library. The statements made herein are solely the responsibility of the authors.

Notes on contributors

Sara I. Ahmad graduated with a Ph.D. from Hamad Bin Khalifa University, Qatar. She is now a post-doctorate fellow at the College of Science and Engineering at Hamad Bin Khalifa University. She mainly focused on the design and manufacturing of nanocomposite materials structures and functions.

Atef Zekri graduated with a PhD in Physics from the University of Oldenburg, Germany. His is currently a Scientist at Qatar Environment and Energy Research Institute, Qatar. His research interests focus on state-of-the-art electron microscopy across a wide range of materials.

Khaled M. Youssef is an associate professor and the director of the Materials Science and Technology Graduate Program at Qatar University, Qatar. Mainly engaged in synthesizing nanomaterials, their properties, and thermal stability.

ORCID

Khaled M. Youssef  <http://orcid.org/0000-0001-9850-5223>

References

1. Smalley M. Survey shows aluminum is a growing automotive material. 2020. Available from: [https://www.aluminum.org/news/survey-reveals-aluminum-](https://www.aluminum.org/news/survey-reveals-aluminum-remains-fastest-growing-automotive-material-emerging-preferred-metal)

2. Fomin EV, Mayer AE, Krasnikov VS. Prediction of shear strength of cluster-strengthened aluminum with multi-scale approach describing transition from cutting to bypass of precipitates by dislocations. *Int J Plast.* 2021;146:103095. doi: [10.1016/j.ijplas.2021.103095](https://doi.org/10.1016/j.ijplas.2021.103095).
3. Polmear IJ. Aluminium alloys – a century of age hardening. *Mater Forum.* 2004;28:1–14.
4. Tisza M, Lukács Z. High strength aluminum alloys in car manufacturing. *IOP Conf Ser Mater Sci Eng.* 2018;418:012033. doi: [10.1088/1757-899X/418/1/012033](https://doi.org/10.1088/1757-899X/418/1/012033).
5. Ahmad SI, Hamoudi H, Abdala A, et al. Graphene-reinforced bulk metal matrix composites: synthesis, microstructure, and properties. *Rev Adv Mater Sci.* 2020;59(1):67–114. doi: [10.1515/rams-2020-0007](https://doi.org/10.1515/rams-2020-0007).
6. Su J, Teng J. Recent progress in graphene-reinforced aluminum matrix composites. *Front Mater Sci.* 2021;15(1):79–97. doi: [10.1007/s11706-021-0541-0](https://doi.org/10.1007/s11706-021-0541-0).
7. Youssef KM, Scattergood RO, Murty KL, et al. Nanocrystalline Al–Mg alloy with ultrahigh strength and good ductility. *Scr Mater.* 2006;54(2):251–256. doi: [10.1016/j.scriptamat.2005.09.028](https://doi.org/10.1016/j.scriptamat.2005.09.028).
8. Petch N. The cleavage strength of polycrystals. *J Iron Steel Inst.* 1953;174:25–28.
9. Khan AS, Zhang H, Takacs L. Mechanical response and modeling of fully compacted nanocrystalline iron and copper. *Int J Plast.* 2000;16(12):1459–1476. doi: [10.1016/S0749-6419\(00\)00023-1](https://doi.org/10.1016/S0749-6419(00)00023-1).
10. Khan AS, Farrokh B, Takacs L. Compressive properties of Cu with different grain sizes: sub-micron to nanometer realm. *J Mater Sci.* 2008;43(9):3305–3313. doi: [10.1007/s10853-008-2508-2](https://doi.org/10.1007/s10853-008-2508-2).
11. Papageorgiou DG, Kinloch IA, Young RJ. Mechanical properties of graphene and graphene-based nanocomposites. *Prog Mater Sci.* 2017;90:75–127. doi: [10.1016/j.pmatsci.2017.07.004](https://doi.org/10.1016/j.pmatsci.2017.07.004).
12. Bisht A, Srivastava M, Kumar RM, et al. Strengthening mechanism in graphene nanoplatelets reinforced aluminum composite fabricated through spark plasma sintering. *Mater Sci Eng A.* 2017;695:20–28. doi: [10.1016/j.msea.2017.04.009](https://doi.org/10.1016/j.msea.2017.04.009).
13. Yolshina LA, Muradymov RV, Korsun IV, et al. Novel aluminum-graphene and aluminum-graphite metallic composite materials: synthesis and properties. *J Alloys Compd.* 2016;663:449–459. doi: [10.1016/j.jallcom.2015.12.084](https://doi.org/10.1016/j.jallcom.2015.12.084).
14. Zhao L, Guo Q, Li Z, et al. Strain-rate dependent deformation mechanism of graphene-Al nanolaminated composites studied using micro-pillar compression. *Int J Plast.* 2018;105:128–140. doi: [10.1016/j.ijplas.2018.02.006](https://doi.org/10.1016/j.ijplas.2018.02.006).
15. Zhao L, Guo Q, Li Z, et al. Strengthening and deformation mechanisms in nanolaminated graphene-Al composite micro-pillars affected by graphene in-plane sizes. *Int J Plast.* 2019;116:265–279. doi: [10.1016/j.ijplas.2019.01.006](https://doi.org/10.1016/j.ijplas.2019.01.006).
16. Bhadauria A, Singh LK, Laha T. Effect of physiochemically functionalized graphene nanoplatelet reinforcement on tensile properties of aluminum nanocomposite synthesized via spark plasma sintering. *J Alloys Compd.* 2018;748:783–793. doi: [10.1016/j.jallcom.2018.03.186](https://doi.org/10.1016/j.jallcom.2018.03.186).

17. Bhadauria A, Singh LK, Nayak SK, et al. Tensile deformation behavior and strengthening mechanism in graphene nanoplatelet reinforced bimodal grained aluminum nanocomposite synthesized by spark plasma sintering and hot rolling. *Mater Charact.* 2020;168:110568. doi: [10.1016/j.matchar.2020.110568](https://doi.org/10.1016/j.matchar.2020.110568).
18. Khanna V, Kumar V, Bansal SA, et al. Fabrication of efficient aluminium/graphene nanosheets (Al-GNP) composite by powder metallurgy for strength applications. *J Mater Res Technol.* 2023;22:3402–3412. doi: [10.1016/j.jmrt.2022.12.161](https://doi.org/10.1016/j.jmrt.2022.12.161).
19. Alizadeh A, Maleki M, Abdollahi A. Preparation of super-high strength nanostructured B4C reinforced Al-2Cu aluminum alloy matrix composites by mechanical milling and hot press method: microstructural, mechanical and tribological characterization. *Adv Powder Technol.* 2017;28(12):3274–3287. doi: [10.1016/j.apt.2017.10.007](https://doi.org/10.1016/j.apt.2017.10.007).
20. Al-Salihi HA, Mahmood AA, Alalkawi HJ. Mechanical and wear behavior of AA7075 aluminum matrix composites reinforced by Al₂O₃ nanoparticles. *Nanocomposites.* 2019;5(3):67–73. doi: [10.1080/20550324.2019.1637576](https://doi.org/10.1080/20550324.2019.1637576).
21. Bhadauria A, Singh LK, Laha T. Combined strengthening effect of nanocrystalline matrix and graphene nanoplatelet reinforcement on the mechanical properties of spark plasma sintered aluminum based nanocomposites. *Mater Sci Eng A.* 2019;749:14–26. doi: [10.1016/j.msea.2019.02.007](https://doi.org/10.1016/j.msea.2019.02.007).
22. Li G, Xiong B. Effects of graphene content on microstructures and tensile property of graphene-nanosheets/aluminum composites. *J Alloys Compd.* 2017;697:31–36. doi: [10.1016/j.jallcom.2016.12.147](https://doi.org/10.1016/j.jallcom.2016.12.147).
23. Yang W, Zhao Q, Xin L, et al. Microstructure and mechanical properties of graphene nanoplates reinforced pure Al matrix composites prepared by pressure infiltration method. *J Alloys Compd.* 2018;732:748–758. doi: [10.1016/j.jallcom.2017.10.283](https://doi.org/10.1016/j.jallcom.2017.10.283).
24. Liu Z-F, Zhang Z-H, Lu J-F, et al. Effect of sintering temperature on microstructures and mechanical properties of spark plasma sintered nanocrystalline aluminum. *Mater Des.* 2014;64:625–630. doi: [10.1016/j.matdes.2014.08.030](https://doi.org/10.1016/j.matdes.2014.08.030).
25. Li H, Zong H, Li S, et al. Uniting tensile ductility with ultrahigh strength via composition undulation. *Nature.* 2022;604(7905):273–279. doi: [10.1038/s41586-022-04459-w](https://doi.org/10.1038/s41586-022-04459-w).
26. Liang F, Zhang B, Yong Y, et al. Enhanced strain delocalization through formation of dispersive micro shear bands in laminated Ni. *Int J Plast.* 2020;132:102745. doi: [10.1016/j.ijplas.2020.102745](https://doi.org/10.1016/j.ijplas.2020.102745).
27. Khan AS, Liu J. A deformation mechanism based crystal plasticity model of ultrafine-grained/nanocrystalline FCC polycrystals. *Int J Plast.* 2016;86:56–69. doi: [10.1016/j.ijplas.2016.08.001](https://doi.org/10.1016/j.ijplas.2016.08.001).
28. Gao X, Yue H, Guo E, et al. Preparation and tensile properties of homogeneously dispersed graphene reinforced aluminum matrix composites. *Mater Des.* 2016;94:54–60. doi: [10.1016/j.matdes.2016.01.034](https://doi.org/10.1016/j.matdes.2016.01.034).
29. Li M, Gao H, Liang J, et al. Microstructure evolution and properties of graphene nanoplatelets reinforced aluminum matrix composites. *Mater Char.* 2018;140:172–178. doi: [10.1016/j.matchar.2018.04.007](https://doi.org/10.1016/j.matchar.2018.04.007).
30. Ahmad SI, Al-Sulaiti LA, Mkhoyan KA, et al. Artifact-free bulk nanocrystalline Al-Li alloys with multiple deformation mechanisms and improved tensile properties. *Mater Today Commun.* 2020;25:101607. doi: [10.1016/j.mtcomm.2020.101607](https://doi.org/10.1016/j.mtcomm.2020.101607).
31. Ahmed SI, Mkhoyan KA, Youssef KM. The activation of deformation mechanisms for improved tensile properties in nanocrystalline aluminum. *Mater Sci Eng A.* 2020;777:139069. doi: [10.1016/j.msea.2020.139069](https://doi.org/10.1016/j.msea.2020.139069).
32. Dixit S, Mahata A, Mahapatra DR, et al. Multi-layer graphene reinforced aluminum – manufacturing of high strength composite by friction stir alloying. *Compos Part B Eng.* 2018;136:63–71. doi: [10.1016/j.compositesb.2017.10.028](https://doi.org/10.1016/j.compositesb.2017.10.028).
33. Li JL, Xiong YC, Wang XD, et al. Microstructure and tensile properties of bulk nanostructured aluminum/graphene composites prepared via cryomilling. *Mater Sci Eng A.* 2015;626:400–405. doi: [10.1016/j.msea.2014.12.102](https://doi.org/10.1016/j.msea.2014.12.102).
34. Rashad M, Pan F, Yu Z, et al. Investigation on microstructural, mechanical and electrochemical properties of aluminum composites reinforced with graphene nanoplatelets. *Progr Nat Sci Mater Int.* 2015;25(5):460–470. doi: [10.1016/j.pnsc.2015.09.005](https://doi.org/10.1016/j.pnsc.2015.09.005).
35. Han T, Wang F, Li J, et al. Simultaneously enhanced strength and ductility of Al matrix composites through the introduction of intragranular nano-sized graphene nanoplates. *Compos Part B Eng.* 2021;212:108700. doi: [10.1016/j.compositesb.2021.108700](https://doi.org/10.1016/j.compositesb.2021.108700).
36. An X, Ni S, Song M, et al. Deformation twinning and detwinning in face-centered cubic metallic materials. *Adv Eng Mater.* 2020;22(1):1900479. doi: [10.1002/adem.201900479](https://doi.org/10.1002/adem.201900479).
37. Bozzolo N, Bernacki M. Viewpoint on the formation and evolution of annealing twins during thermomechanical processing of FCC metals and alloys. *Metall Mater Trans A.* 2020;51(6):2665–2684. doi: [10.1007/s11661-020-05772-7](https://doi.org/10.1007/s11661-020-05772-7).
38. Zhang Y, Tao NR, Lu K. Effects of stacking fault energy, strain rate and temperature on microstructure and strength of nanostructured Cu–Al alloys subjected to plastic deformation. *Acta Mater.* 2011;59(15):6048–6058. doi: [10.1016/j.actamat.2011.06.013](https://doi.org/10.1016/j.actamat.2011.06.013).
39. Zhang L, Shibuta Y, Huang X, et al. Grain boundary induced deformation mechanisms in nanocrystalline Al by molecular dynamics simulation: from interatomic potential perspective. *Comput Mater Sci.* 2019;156:421–433. doi: [10.1016/j.commatsci.2018.10.021](https://doi.org/10.1016/j.commatsci.2018.10.021).
40. Muzyk M, Pakieła Z, Kurzydłowski KJ. Generalized stacking fault energies of aluminum alloys—density functional theory calculations. *Metals.* 2018;8(10):823. doi: [10.3390/met8100823](https://doi.org/10.3390/met8100823).
41. Zhu L, Li N, Childs PRN. Light-weighting in aerospace component and system design. *Propul Power Res.* 2018;7(2):103–119. doi: [10.1016/j.jppr.2018.04.001](https://doi.org/10.1016/j.jppr.2018.04.001).
42. Klug HP, Alexander LE. X-ray diffraction procedures for polycrystalline and amorphous materials. 2nd ed. New York: John Wiley & Sons; 1974.
43. El-Ghazaly A, Anis G, Salem HG. Effect of graphene addition on the mechanical and tribological behavior of nanostructured AA2124 self-lubricating metal matrix composite. *Compos Part A Appl Sci*

- Manuf. 2017;95:325–336. doi: [10.1016/j.compositesa.2017.02.006](https://doi.org/10.1016/j.compositesa.2017.02.006).
44. Zhang H, Xu C, Xiao W, et al. Enhanced mechanical properties of Al5083 alloy with graphene nanoplates prepared by ball milling and hot extrusion. *Mater Sci Eng A*. 2016;658:8–15. doi: [10.1016/j.msea.2016.01.076](https://doi.org/10.1016/j.msea.2016.01.076).
 45. Singh LK, Bhadauria A, Laha T. Comparing the strengthening efficiency of multiwalled carbon nanotubes and graphene nanoplatelets in aluminum matrix. *Powder Technol*. 2019;356:1059–1076. doi: [10.1016/j.powtec.2019.09.026](https://doi.org/10.1016/j.powtec.2019.09.026).
 46. Tiwari JK, Mandal A, Rudra A, et al. Influence of graphene content on the mechanical properties of severely deformed graphene/aluminum composite. *Mater Chem Phys*. 2020;248:122939. doi: [10.1016/j.matchemphys.2020.122939](https://doi.org/10.1016/j.matchemphys.2020.122939).
 47. Ferrari AC, Meyer JC, Scardaci V, et al. Raman spectrum of graphene and graphene layers. *Phys Rev Lett*. 2006;97(18):187401. doi: [10.1103/PhysRevLett.97.187401](https://doi.org/10.1103/PhysRevLett.97.187401).
 48. El-Makaty FM, Ahmed HK, Youssef KM. Review: the effect of different nanofiller materials on the thermoelectric behavior of bismuth telluride. *Mater Des*. 2021;209:109974. doi: [10.1016/j.matdes.2021.109974](https://doi.org/10.1016/j.matdes.2021.109974).
 49. Yue H, Yao L, Gao X, et al. Effect of ball-milling and graphene contents on the mechanical properties and fracture mechanisms of graphene nanosheets reinforced copper matrix composites. *J Alloys Compd*. 2017;691:755–762. doi: [10.1016/j.jallcom.2016.08.303](https://doi.org/10.1016/j.jallcom.2016.08.303).
 50. Kumar KS, Suresh S, Chisholm MF, et al. Deformation of electrodeposited nanocrystalline nickel. *Acta Mater*. 2003;51(2):387–405. doi: [10.1016/S1359-6454\(02\)00421-4](https://doi.org/10.1016/S1359-6454(02)00421-4).
 51. Balan KP. Chapter two - fracture. In: Balan KP, editor. *Metallurgical failure analysis*. Amsterdam, Netherlands: Elsevier; 2018. p. 7–16.
 52. Avramovic-Cingara G, Saleh C, Jain MK, et al. Void nucleation and growth in dual-phase steel 600 during uniaxial tensile testing. *Metall Mater Trans A*. 2009;40(13):3117–3127. doi: [10.1007/s11661-009-0030-z](https://doi.org/10.1007/s11661-009-0030-z).
 53. Tian W-M, Li S-M, Wang B, et al. Graphene-reinforced aluminum matrix composites prepared by spark plasma sintering. *Int J Miner Metall Mater*. 2016;23(6):723–729. doi: [10.1007/s12613-016-1286-0](https://doi.org/10.1007/s12613-016-1286-0).
 54. Khan M, Ud Din R, Wadood A, et al. Effect of graphene nanoplatelets on the physical and mechanical properties of Al6061 in fabricated and T6 thermal conditions. *J Alloys Compd*. 2019;790:1076–1091. doi: [10.1016/j.jallcom.2019.03.222](https://doi.org/10.1016/j.jallcom.2019.03.222).
 55. Sun W, Zhan K, Yang Z, et al. Facile fabrication of GO/Al composites with improved dispersion of graphene and enhanced mechanical properties by Cu doping and powder metallurgy. *J Alloys Compd*. 2020;815:152465. doi: [10.1016/j.jallcom.2019.152465](https://doi.org/10.1016/j.jallcom.2019.152465).
 56. Ismail E, Fauzi FB, Mohamed MA, et al. Kinetic studies of few-layer graphene grown by flame deposition from the perspective of gas composition and temperature. *RSC Adv*. 2019;9(36):21000–21008. doi: [10.1039/c9ra01257e](https://doi.org/10.1039/c9ra01257e).
 57. Gürbüz M, Can Şenel M, Koç E. The effect of sintering time, temperature, and graphene addition on the hardness and microstructure of aluminum composites. *J Compos Mater*. 2017;52(4):553–563. doi: [10.1177/0021998317740200](https://doi.org/10.1177/0021998317740200).
 58. Hu Z, Chen F, Xu J, et al. 3D printing graphene-aluminum nanocomposites. *J Alloys Compd*. 2018;746:269–276. doi: [10.1016/j.jallcom.2018.02.272](https://doi.org/10.1016/j.jallcom.2018.02.272).
 59. Liu X, Li J, Liu E, et al. Towards strength-ductility synergy with favorable strengthening effect through the formation of a quasi-continuous graphene nanosheets coated Ni structure in aluminum matrix composite. *Mater Sci Eng A*. 2019;748:52–58. doi: [10.1016/j.msea.2019.01.046](https://doi.org/10.1016/j.msea.2019.01.046).
 60. Xiong B, Liu K, Yan Q, et al. Microstructure and mechanical properties of graphene nanoplatelets reinforced Al matrix composites fabricated by spark plasma sintering. *J Alloys Compd*. 2020;837:155495. doi: [10.1016/j.jallcom.2020.155495](https://doi.org/10.1016/j.jallcom.2020.155495).
 61. Zhou W, Fan Y, Feng X, et al. Creation of individual few-layer graphene incorporated in an aluminum matrix. *Compos Part A Appl Sci Manuf*. 2018;112:168–177. doi: [10.1016/j.compositesa.2018.06.008](https://doi.org/10.1016/j.compositesa.2018.06.008).
 62. Pérez-Bustamante R, Bolaños-Morales D, Bonilla-Martínez J, et al. Microstructural and hardness behavior of graphene-nanoplatelets/aluminum composites synthesized by mechanical alloying. *J Alloys Compd*. 2014;615:S578–S582. doi: [10.1016/j.jallcom.2014.01.225](https://doi.org/10.1016/j.jallcom.2014.01.225).
 63. Li J, Zhang X, Geng L. Effect of heat treatment on interfacial bonding and strengthening efficiency of graphene in GNP/Al composites. *Compos Part A Appl Sci Manuf*. 2019;121:487–498. doi: [10.1016/j.compositesa.2019.04.010](https://doi.org/10.1016/j.compositesa.2019.04.010).
 64. Gleiter H. Nanocrystalline materials. *Prog Mater Sci*. 1989;33(4):223–315. doi: [10.1016/0079-6425\(89\)90001-7](https://doi.org/10.1016/0079-6425(89)90001-7).
 65. Suryanarayana C. Nanocrystalline materials. *Int. Mater. Rev*. 1995;40(2):41–64. doi: [10.1179/imr.1995.40.2.41](https://doi.org/10.1179/imr.1995.40.2.41).
 66. Zhang L, Mao W, Liu M, et al. Mechanical response and plastic deformation of coherent twin boundary with perfect and defective structures. *Mech Mater*. 2020;141:103266. doi: [10.1016/j.mechmat.2019.103266](https://doi.org/10.1016/j.mechmat.2019.103266).
 67. Nardone VC, Prewo KM. On the strength of discontinuous silicon carbide reinforced aluminum composites. *Scr Metall*. 1986;20(1):43–48. doi: [10.1016/0036-9748\(86\)90210-3](https://doi.org/10.1016/0036-9748(86)90210-3).
 68. Guo Y, Yi D, Liu H, et al. Mechanical properties and conductivity of graphene/Al-8030 composites with directional distribution of graphene. *J Mater Sci*. 2020;55(8):3314–3328. doi: [10.1007/s10853-019-04017-2](https://doi.org/10.1007/s10853-019-04017-2).
 69. Jin J, Wang L, Zheng Z, et al. Metal-insulator-metal diodes based on alkyltrichlorosilane self-assembled monolayers. *AIP Adv*. 2019;9(6):065017. doi: [10.1063/1.5100252](https://doi.org/10.1063/1.5100252).
 70. Zhou W, Mikulova P, Fan Y, et al. Interfacial reaction induced efficient load transfer in few-layer graphene reinforced Al matrix composites for high-performance conductor. *Compos Part B Eng*. 2019;167:93–99. doi: [10.1016/j.compositesb.2018.12.018](https://doi.org/10.1016/j.compositesb.2018.12.018).
 71. Xiong B, Liu K, Xiong W, et al. Strengthening effect induced by interfacial reaction in graphene nanoplatelets reinforced aluminum matrix composites. *J Alloys Compd*. 2020;845:156282. doi: [10.1016/j.jallcom.2020.156282](https://doi.org/10.1016/j.jallcom.2020.156282).
 72. Li Z, Fu X, Guo Q, et al. Graphene quality dominated interface deformation behavior of graphene-

- metal composite: the defective is better. *Int J Plast.* 2018;111:253–265. doi: [10.1016/j.ijplas.2018.07.020](https://doi.org/10.1016/j.ijplas.2018.07.020).
73. Demir E, Gutierrez-Urrutia I. Investigation of strain hardening near grain boundaries of an aluminum oligocrystal: experiments and crystal based finite element method. *Int J Plast.* 2021;136:102898. doi: [10.1016/j.ijplas.2020.102898](https://doi.org/10.1016/j.ijplas.2020.102898).
 74. Linne MA, Bieler TR, Daly S. The effect of microstructure on the relationship between grain boundary sliding and slip transmission in high purity aluminum. *Int J Plast.* 2020;135:102818. doi: [10.1016/j.ijplas.2020.102818](https://doi.org/10.1016/j.ijplas.2020.102818).
 75. Bao H, Xu H, Li Y, et al. The interaction mechanisms between dislocations and nano-precipitates in CuFe alloys: a molecular dynamic simulation. *Int J Plast.* 2022;155:103317. doi: [10.1016/j.ijplas.2022.103317](https://doi.org/10.1016/j.ijplas.2022.103317).
 76. Arsenault RJ, Shi N. Dislocation generation due to differences between the coefficients of thermal expansion. *Mater Sci Eng.* 1986;81:175–187. doi: [10.1016/0025-5416\(86\)90261-2](https://doi.org/10.1016/0025-5416(86)90261-2).
 77. Liao XZ, Zhou F, Lavernia EJ, et al. Deformation twins in nanocrystalline Al. *Appl Phys Lett.* 2003; 83(24):5062–5064. doi: [10.1063/1.1633975](https://doi.org/10.1063/1.1633975).
 78. Beyerlein IJ, Zhang X, Misra A. Growth twins and deformation twins in metals. *Annu Rev Mater Res.* 2014;44(1):329–363. doi: [10.1146/annurev-matsci-070813-113304](https://doi.org/10.1146/annurev-matsci-070813-113304).
 79. Liu L, Zhang Y, Li J, et al. Enhanced strength-ductility synergy via novel bifunctional nano-precipitates in a high-entropy alloy. *Int J Plast.* 2022;153: 103235. doi: [10.1016/j.ijplas.2022.103235](https://doi.org/10.1016/j.ijplas.2022.103235).
 80. Li M, Wang Y, Gao H, et al. Thermally stable microstructure and mechanical properties of graphene reinforced aluminum matrix composites at elevated temperature. *J Mater Res Technol.* 2020; 9(6):13230–13238. doi: [10.1016/j.jmrt.2020.09.068](https://doi.org/10.1016/j.jmrt.2020.09.068).
 81. Li M, Zhang Z, Gao H, et al. Formation of multi-layer interfaces and the load transfer in graphene nanoplatelets reinforced Al matrix composites. *Mater Charact.* 2020;159:110018. doi: [10.1016/j.matchar.2019.110018](https://doi.org/10.1016/j.matchar.2019.110018).
 82. Liu Y, Zhang J, Zhao L, et al. Helium-bubble-assisted deformation twinning in irradiated graphene (reduced graphene oxide)-aluminum composite with a nanolaminated structure. *J Nucl Mater.* 2021;545:152741. doi: [10.1016/j.jnucmat.2020.152741](https://doi.org/10.1016/j.jnucmat.2020.152741).
 83. Li Q, Cho J, Xue S, et al. High temperature thermal and mechanical stability of high-strength nano-twinned Al alloys. *Acta Mater.* 2019;165:142–152. doi: [10.1016/j.actamat.2018.11.011](https://doi.org/10.1016/j.actamat.2018.11.011).
 84. Yang W, Dong R, Jiang L, et al. Unstable stacking faults in submicron/micron Al grammings in multi-SiCp/multi-Al nanocomposite. *Vacuum.* 2015;122: 1–5. doi: [10.1016/j.vacuum.2015.09.002](https://doi.org/10.1016/j.vacuum.2015.09.002).
 85. Li Z, Zhao S, Alotaibi SM, et al. Adiabatic shear localization in the CrMnFeCoNi high-entropy alloy. *Acta Mater.* 2018;151:424–431. doi: [10.1016/j.actamat.2018.03.040](https://doi.org/10.1016/j.actamat.2018.03.040).
 86. Zhou F, Liao XZ, Zhu YT, et al. Microstructural evolution during recovery and recrystallization of a nanocrystalline Al-Mg alloy prepared by cryogenic ball milling. *Acta Mater.* 2003;51(10):2777–2791. doi: [10.1016/S1359-6454\(03\)00083-1](https://doi.org/10.1016/S1359-6454(03)00083-1).
 87. Guo B, Song M, Zhang X, et al. Exploiting the synergic strengthening effects of stacking faults in carbon nanotubes reinforced aluminum matrix composites for enhanced mechanical properties. *Compos Part B Eng.* 2021;211:108646. doi: [10.1016/j.compositesb.2021.108646](https://doi.org/10.1016/j.compositesb.2021.108646).
 88. Zheng Z, Zhong S, Zhang X, et al. Graphene nanoplatelets reinforced aluminum composites with anisotropic compressive properties. *Mater Sci Eng A.* 2020;798:140234. doi: [10.1016/j.msea.2020.140234](https://doi.org/10.1016/j.msea.2020.140234).
 89. Shin SE, Ko YJ, Bae DH. Mechanical and thermal properties of nanocarbon-reinforced aluminum matrix composites at elevated temperatures. *Compos Part B Eng.* 2016;106:66–73. doi: [10.1016/j.compositesb.2016.09.017](https://doi.org/10.1016/j.compositesb.2016.09.017).
 90. Asgharzadeh H, Sedigh M. Synthesis and mechanical properties of Al matrix composites reinforced with few-layer graphene and graphene oxide. *J Alloys Compd.* 2017;728:47–62. doi: [10.1016/j.jallcom.2017.08.268](https://doi.org/10.1016/j.jallcom.2017.08.268).